Information Content of Very High Resolution SAR Images: Study of Dependency of SAR Image Structure Descriptors with Incidence Angle

Corneliu Octavian Dumitru
Remote Sensing Technology Institute (IMF)
German Aerospace Center (DLR)
Oberpfaffenhofen – Wessling, Germany
corneliu.dumitru@dlr.de

Mihai Datcu
Remote Sensing Technology Institute (IMF)
German Aerospace Center (DLR)
Oberpfaffenhofen – Wessling, Germany
mihai.datcu@dlr.de

***Abstract*—This paper provide systematic results of the influence of the Synthetic Aperture Radar image structure descriptors with incidence angle and orbit direction. The evaluation is done on TerraSAR-X data and the interpretation is done semi-automatically. In the first part, we study and assess the behavior of the primitive feature extracted methods for images of the same scene with 2 look angles covering the min-max range of the sensor. After that the influence of the orbit looking is shortly discuss. The tests are done on TerraSAR-X products High Resolution Spotlight mode at 3 m resolution and two sites covering the Berlin and Ottawa area are found to be suitable for this investigation. To identify the best features and appropriate incidence angle for them the Support Vector Machine and as a measure of the classification accuracy the precision–recall were considered. The recall shows that the optimal value of the incidence angle in order to have a higher classification is obtained for a value of the incidence angle closer to upper bound of the sensor range. In the second part of the paper a list of queries that can be asked by Earth Observation users are presented and proposed to be implemented in the next generation of our system. The first contribution of this paper is the evaluation of four primitive features that are very known (gray level co-occurrence matrix, Gabor filter, quadrature mirror filter, and non-linear short time Fourier transform) but not used and compared for SAR images. After the best primitive feature is identified the second contribution of this paper lies in the fact that the parameters of the data namely, incidence angle and orbit direction are systematically investigated in order to find the dependency between these parameters and the accuracy of the retrieved classes.**

Keywords-classes; features; inicdence angle; orbit direction; query; SAR iamges

I. INTRODUCTION

The specific information in High Resolution (HR) Synthetic Aperture Radar (SAR) images acquired in single polarization is mainly in the "structure", e.g. textures, objects, or scattering signatures. The "spatial context" becomes very important rather than the "pixel based" descriptors, which are less informational. The adopted solution is to analyze image patches corresponding to ground areas of ca. 200 x 200m. Experiments and tests carried recently confirmed the usefulness of the concept, however further analysis is needed to assess the behavior of the method for the indexing of very large SAR data sets as the case in Image Information Mining (IIM) [1].

There are few publications available [2] ÷ [6] where the images are tiled into patches and generating a large number of classes. In [2], the patch size is 256 x 256m in order to ensure that the extracted information capture the local characteristics within a patch rather the global features across the entire image.

In [3], the TerraSAR-X high resolution Spotlight products (resolution of ~1 m) were tiled into patches of 200 x 200m in order to characterize the large and relatively small structures available in the urban scene. The images covered different region: Las Vegas, Venice, Gizah, and Gauting. From 7,000 extracted patches a set of 30 classes were generated.

In [4], the original images are tiled into patches of 16 x 16 pixels or 128 x 128 pixels. Three classes were extracted (city, forest, and sea) and the results of the classification shows better performances when the image was tiled in patches of 128 x 128 pixels. The same authors propose in [5] a patch contextual approach for high resolution satellite images (resolution of 0.6 m) where the patch size is 200 x 200 pixels. The number of classes was 18.

In our previous work [6], a pyramid with different resolutions (1m, 2m, 2.9m, 4m, and 8m) was considered for TerraSAR-X high resolution Spotlight where each image was tiled into patches at different size in order to have the same area covered on the ground. The patch sizes vary from 400 x 400m (for 1m resolution) to 25 x 25m (for 8m resolution). The two scenes (Venice and Toulouse) were considered for this investigation and 30 classes were identified.

In this paper, we propose to study and experimentally asses the most relevant PF behavior for indexing the content of SAR images as TerraSAR-X. The envisaged algorithms

are very well known but not very used for SAR data. After finding the best primitive feature algorithm considering the optimal size of the patch for high resolution Spotlight mode radiometrically enhanced product equal to 220 x 220 pixels the second step was to determine the dependency of the SAR imaging with the incidence angle. In the end of the paper a series of queries that can implemented starting from the TerraSAR-X metadata (available in the XML file attached to the product), TerraSAR-X image, patches, semantic annotation (ontology) of the patches, and primitive features extracted from each patch were presented.

The paper structure is the following. Section II presents the TerraSAR-X products used for tests and based on this a test dataset is built. Section III explains the actual state-of-the-art of the feature extraction methods and shortly describes the applied methods. Section IV describes the methodology used in the next Section. Section V provides the details about the experiments, while Section VI gives some examples of queries that can be implemented in EO systems. Section VII points the conclusion and references given at the end of the paper.

II. TERRASAR-X PRODUCTS

In this section, we discuss the basic TerraSAR-X products that are intend to be used and the *test dataset* that was built for this evaluation.

TerraSAR-X is the German radar satellite and it operates in the X-band with a side-looking SAR based on active phased array antenna technology [7]. It does supply high quality radar data for purposes of scientific observation of the Earth.

The basic products [7] are available in a huge diversity of modes (Stripmap, Spotlight, ScanSAR), types (complex, detected, geocoded), and configurations (Spatially Enhanced Products or Radiometrically Enhanced Products).

In Figure 1, examples of the basic products are presented in order to understand the diversity of TerraSAR-X satellite and the difference between these products. Note that, in the examples shown in Figure 1, the ScanSAR mode and SSC type are missing because was not possible to find in the archive these products covering the same area of interest.

The size of the sub-images tiled from the original image and presented in Figure 1 is the same but the coverage on the ground is different because the resolution and/or pixel spacing of this is different.

From this huge diversity of products we selected based on our previous results [6], [34], and [37] the following configuration:

- the high resolution Spotlight (HS) mode as one of the most popular mode used for research,
- the detected product GEC (Geo-coded Elipsoid Corrected) products because is geo-referenced product and the localisation of the pixels can be realised with a higher accuracy than for other products. In some applications this is very important.
- the radiometrically enhanced (RE) configuration where the range and azimuth resolution are decreased in order to reduce the speackle.

Our *test dataset* is created in order to answer to the following question: "*Which is the optimal incidence angle for a better classification?*".

The characteristics of the *test dataset* (configuration of the product presented before) that we identified in the TerraSAR-X archive [34] and selected for this evaluation (Berlin – Germany and Ottawa – Canada) are the following:

- the ground range resolution is about 2.9 meters,
- the single polarisation HH,

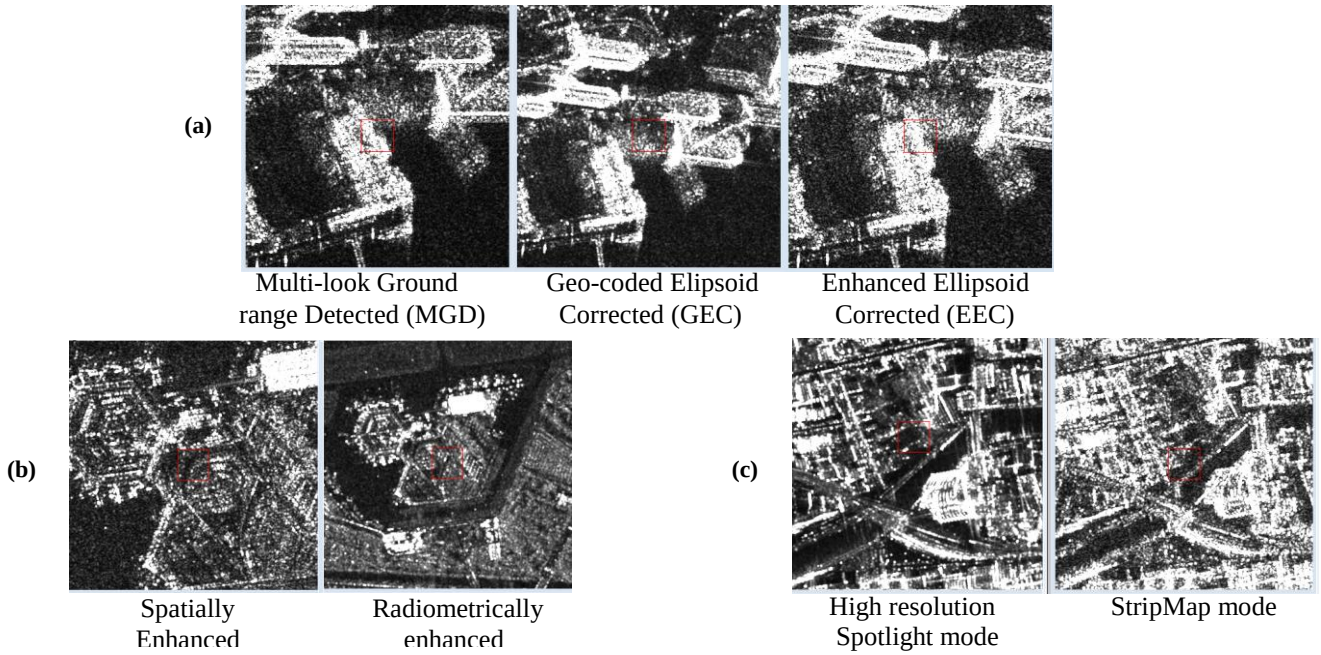

Figure 1. Comparative examples of TerraSAR-X products that covers the diversity of: (a) types, (b) geometric resolution configurations, and (c) modes.

- the orbit looking is ascending for Berlin and descending for Ottawa,
- the incidence angle is 30° and 42° for Berlin and 27° and 41° for Ottawa,
- the number of looks depends by the incidence angle and varies from 5 for an incidence angle of 20° to 9 for an incidence angle of 55°,
- the size of the images is 5549 x 3368 pixels in case of Berlin and 4783 x 3381 pixels in case of Ottawa. From the image a rectangle is selected in order to not have the black letter box effect on the processing of the features (see Figure 10).

In order to understand the difference between different values of the incidence angle in Figure 2-a two examples are presented. The first one corresponds to central station in Berlin and the acquisition of the data was different in order to cover the range of the incidence angle. The second one corresponds to high builds in the financial district of Ottawa and also here the incidence angle was different in order to capture the sensibility of the data with the incidence angle.

Similar examples are presented in Figure 2-b but this time we are interested in the orbit direction and for this reason we selected two area in Berlin having the orbit direction ascending and descending.

For high resolution SAR images the diversity of the classes that can be retrieved from the image is higher than in the case of lower resolution images. In Figure 3 the diversity of the classes identified in our *test dataset* is shown.

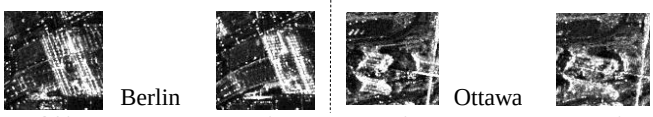

Figure 2-a. Different patches tiled from the images having the incidence angle close to lower and upper bound of the sensor range for Berlin (left side of the image) and Ottawa (right side of the image). The characteristics of the entire image from where the patches were tiled are: TerraSAR-X HS mode with RE configuration at about 2.9 meters resolution with ascending looking for Berlin and descending looking for Ottawa.

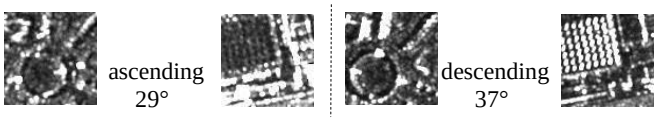

Figure 2-b. Examples of patches covering the same area on ground but with a different orbit direction and incidence angle for the area of Berlin. The characteristics of the image from where the patches were tiled are: TerraSAR-X HS mode with RE configuration at 6.5 meters resolution.

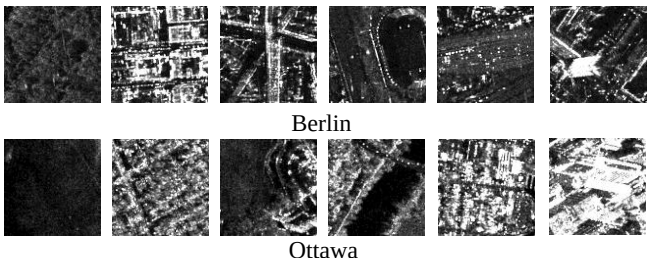

Figure 3. A set of classes that can be extracted from the two investigate sites that are available in our *test dataset*.

III. FEATURES EXTRACTION METHODS

In this section, we select four feature extraction methods that have been proposed in the past several decades by different authors and we compare these for SAR images.

On a conceptual level we decide which features can be extracted in general and on a practical level, we apply the: gray level co-occurrence feature extraction [13] for texture analysis, Gabor filtering [18] to extract any geometrical or neighborhood relationships, quadrature mirror filters [30] for texture analysis, and non-linear short time Fourier transform [32] for spectral characteristics of the image.

We can divide the features in two categories: statistical and spectral [27], [28].

A. Statistical

1) Gray level co-occurrence matrix

a) State of the art

The gray level co-occurrence matrix (GLCM) is a second order statics of how often different combinations of pixel brightness values (gray levels) occur in an image [13].

Haralick et al. [8] compute gray level co-occurrence matrix for a distance of one with four directions (0°, 45°, 90°, and 135°). For a seven-class classification problem, they obtained approximately 80% classification accuracy using texture features in remote sensing images application.

Rignot and Kwok [9] have analyzed SAR images using texture features computed from GLCM. However, they supplement these features with knowledge about the properties of SAR images. For example, image restoration algorithms were used to eliminate the specular noise present in SAR images in order to improve classification results.

Schistad and Jain [10] compare different methods for texture computation in ERS SAR imagery. One of the used and computed methods was GLCM with four directions like in [8]. The *angular second moment, contrast, entropy, cluster shade, inertia, and inverse difference moment* [13] were computed as texture features from the GLCM. A five class classification problem was considered and 29% (an average) classification error using GLCM was obtained.

Randen and Husoy [11] consider GLCM as a reference method and they compared this with other filtering methods (like: QMF, Gabor, discrete cosine transform, etc.) for texture extraction. The size of the gray levels in the image is 8 x 8 (also chosen by Ohanian and Dubes [12]). On the one hand, if the value is large, the number of pixel pairs contributing to each element in image will be low, and the statistical significance poor. On the other hand, if the gray levels are low, much of the texture information may be lost in the image quantization. The *angular second moment, contrast, correlation, and entropy* were computed as texture features for each orientation. The average of the classification error was 32%.

b) Appplied method

The GLCM is created from a gray scale image by selecting either horizontal (0°), vertical (90°), or diagonal (45° or 135°) orientation.

The size of GLCM depends on the number of gray values available in the image. For example, in [29], they obtain for

an input image of 8 bits, i.e., 256 values, a GLCM of 256x256 elements.

In our case, we scale the radiometric range of the input images to 16 steps and obtain a GLCM size of 16x16 elements.

The texture parameters [13] computed from the GLCM are: *mean*, *variance*, *entropy*, *contrast*, *energy*, *correlation*, *homogeneity*, *autocorrelation*, *dissimilarity*, *cluster shade*, *cluster prominence*, and *maximum probability*.

B. Spectral

1) Gabor filters

a) State of the art

A Gabor filter is a linear filter used in image processing that is included as a descriptor in MPEG 7 [38].

Randen and Husoy [11] review the major filtering approaches to texture feature extraction and performed a comparative study by comparing with two classical non-filtering approaches (GLCM which is a statistical method and autoregressive which is model based method). The dyadic Gabor filter bank (i.e. Gaussian shaped band-pass filters, with dyadic coverage of the radial spatial frequency range and multiple orientations) proposed by Jain and Farrokhnia [14] was considered for the experiments in [11]. Five radial frequency were used (proposed by [14] for images of size 256 x 256 pixels) and four orientations (0°, 45°, 90°, and 135°). The average error on the classification was 31%.

Du [15] used texture features derived from Gabor filters to segment SAR images. He successfully segmented the SAR images into classes of water, new forming ice, older ice, and multi-year ice. Lee and Philpot [16] also used spectral texture features to segment SAR images.

Shu et al. [17] extract the information at four directions (0°, 45°, 90°, and 135°) by using Gabor filters and then computing the mutual information of each corresponding image pair. The experiments show that the method can work very well even if the SAR image is not filtered; this indicates that the method is robust to speckle noise.

In Manjunath and Ma [18], a Gabor wavelet based texture analysis method is proposed and its application to image databases is demonstrated on Brodatz texture database but also considering the current work related to the idea of browsing large satellite images database. The experiments results demonstrate that these Gabor features are robust. Rotation and scale invariance are important in many applications and the preliminary results obtained by [18] using Gabor features are very promising.

In [19] ÷ [22], the Gabor filters are applied to Brodatz texture database with very good results.

b) Appplied method

Frequency and orientation representations of a Gabor filter are similar to those of the human visual system, and it has been found to be particularly appropriate for texture representation and discrimination. In the spatial domain, a 2D Gabor filter is a Gaussian kernel function modulated by a sinusoidal plane wave [18]. The Gabor filters are self-similar - all filters can be generated from one mother wavelet by dilation and rotation.

We have chosen the Gabor filters designed by Manjunath B.S. and Ma W.Y. at Vision Research Lab, University of California.

The texture parameter results computed from the Gabor filter are *mean* and *variance* for different *scales* and *orientations*.

2) Quadrature mirror filters

a) State of the art

Quadrature Mirror Filter (QMF) banks are multirate (i.e. with variable sampling rate throughout the system) digital filter banks, introduced by Croisier, [23], Esteban and Galand [24]. During the last two decades since the inception of QMF banks, they have been extensively used in speech signal processing, image processing and digital transmultiplexers [25]. QMF banks are used to split a discrete-time signal into a number of bands in the frequency domain to process each sub-band in independent manner.

QMF was used for texture analysis by Randen and Husoy [11] as extended classes of filters which include among others Gabor filters, discrete cosine transform, etc. This is a large class of filters which incorporate both infinite impulse response (IIR) and finite impulse response (FIR) filters. In their experiments the average of the classification error was between 26% and 33%.

b) Appplied method

As proposed in [30], statistical features obtained from the filtered images using QMF banks in synergy with some other features can be used for image (satellite image) indexing.

The number of features which can be obtained from the presented algorithm depends upon the level selected for the QMF sub-band decomposition like a wavelet. Features are nothing but the mean and variance of the four filtered and sub-sampled images in the QMF sub-band pyramid.

There are many techniques available to design QMF banks. We have chosen the QMF banks designed by Simoncelli E.P.and Adelson E.H. at the Vision Science Group, The Media Laboratory, Massachusetts Institute of Technology.

The parameters computed from the QMF banks (QMFS) are *mean* and *variance* of the *low pass sub-band*, *horizontal sub-band*, *vertical sub-band*, and *diagonal sub-band*.

3) Non-linear short time Fourier transform

a) State of the at

Much work on extraction of features based on short time Fourier transform is done in speech and audio processing.

The method proposed in [26] was investigated by Li and Ogihara [32] for music information retrieval. They are using short time Fourier transform feature extraction method to extract the timbral texture witch is not capture by the popular method in speech and music processing, the Mel-frequency cepstral coefficients. The derived features computed from STFT are: spectral centroid, spectral Rolloff, spectral flux, low energy, and zero crossings.

The goal of Popescu et al. paper [26] is to define an analysis model for High Resolution Spotlight SAR imagery, which is able to integrate the radiometric, as well as

geometric and texture properties of the SAR data, in order to facilitate large data-base queries by informational content indexing of the images. The proposed model use the information contained in the spectra of the SAR signal.

The Short Time Fourier Transform (STFT) was considered in order to extract the features necessary for the Bayesian Support Vector Machine classifier. The features are: spectral centroid, spectral flux, cepstral coefficients, and first and second statistic measures. Using this method a number of 30 classes were recognized from the 9,000 patches of SAR images acquired with TerraSAR-X satellite.

b) Appplied method

This method of SAR image feature extraction and complex image information retrieval was first proposed in [31]. This non-parametric analysis is a form of time frequency analysis where the cutting of a spectrum allows the study of the phase responses of scatterers seen from different viewing angles.

The STFT extracts six non-linear features: the first two features are based on statistical properties of the spectrum and the next four features are timbre features used for music genre classification [32].

Non-linear STFT (NLFT) features were initially proposed mainly for feature extraction from complex-valued SAR images, but experiments showed that they give very encouraging results also for real-valued images.

Our proposed algorithm is an implementation of the non-linear STFT feature extraction. The features parameters computed from the STFT are: *mean* of the STFT coefficients, *variance* of the STFT coefficients, *spectral centroid in range*, *spectral centroid in azimuth*, *spectral flux in range*, and *spectral flux in azimuth*.

IV. METHODOLOGY

In this section is presented the methodology used in order to identify the best primitive feature (PF) and the incidence angle /orbit direction that has a good classification accuracy of the TerraSAR-X.

The general approach adopted here is to divide the TerraSAR-X image into a number of sub-images (by tiling the image into patches) [6] and to compute the feature extraction associated to these patches.

For our investigation two sites were considered covering the area of Berlin (Germany) and Ottawa (Canada).

First step is the evaluation of the best primitive features (GLCM, GAFS, QMFS, and NLFT); features extracted using as a test data the Berlin image. The second step of our evaluation is to try to identify the incidence angle and orbit direction that gives a better accuracy of the classification using the best primitive feature identified during the previous step. The evaluation of the second step is done on both sites available in the *test dataset*, Berlin and Ottawa.

To answer to the two questions regarding the best PF and incidence angle / orbit direction of the TerraSAR-X a tool based on Support Vector Machine with relevance feedback (SVM – RF) was built [6].

The SVM – RF tool supports users to search patches of interest in a large database. The Graphical User Interface of this tool allows Human-Machine Interaction to rank the automatically suggested patches which are expected to be grouped in classes. Visual supported ranking allows enhancing the quality of search results by giving positive and negative examples.

The TerraSAR-X product-image is tiled into patches with the size of 220 x 220 meters, and after that are sub-sampled to 110 x 110 meters for better performances (see reference [39] where comparative results are presented in order to find the optimal patch size).

The feature vector for GLCM has a fix number of parameters for each orientation equal to 12, but in order to capture the information of the object orientation all four orientations (from 1 to 4) of GLCM are taking into account (48 components denoted by GLCM_1_2_3_4). In the case of Gabor filters, 4 scales and 6 orientations (48 features denoted by GAFS 4_6) were considered. For QMFS, the number of levels of wavelet decomposition was set equal to 1 this means a vector of 8 features was obtained (denoted by QMFS 1). The last feature vector is represented by NLFT and the number of features was fixed to 6.

All the features are normalised before being used in the SVM-RF tool. The Z-score normalisation method was selected and used from the methods available in [33].

We define a number of semantic classes and group the patches accordingly, using the SVM-RF tool (see the flowchart in Figure 4) and the human expertise (using as a ground truth the Google Earth. We considered that a patch belong to only one class based on the dominant content of the patch.

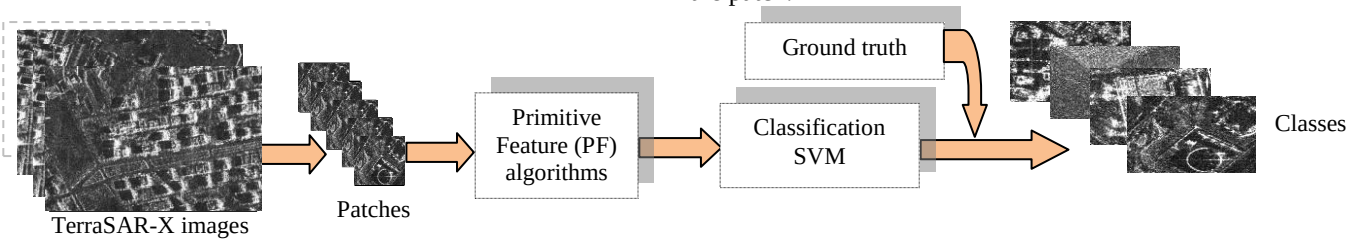

Figure 4. The proposed methodology is the following: (1) the input SAR images are tiled into patches at different size (depending by the resolution and pixel spacing of the image) and the primitive features (GLCM_1_2_3_4, GAFS 4_6, QMFS 1, and NLFT) are computed for each patch; (2) the features are grouped in classes using the Support Vector Machine classifier; (3) the Google Earth is used as a ground truth in order to define the semantic of the generated classes and for visual inspection of these classes. For the evaluation of the best PF the precision-recall metric is computed and after that the PF algorithm having the highest recall is used for the evaluation of the incidence angle and orbit direction following the same procedure.

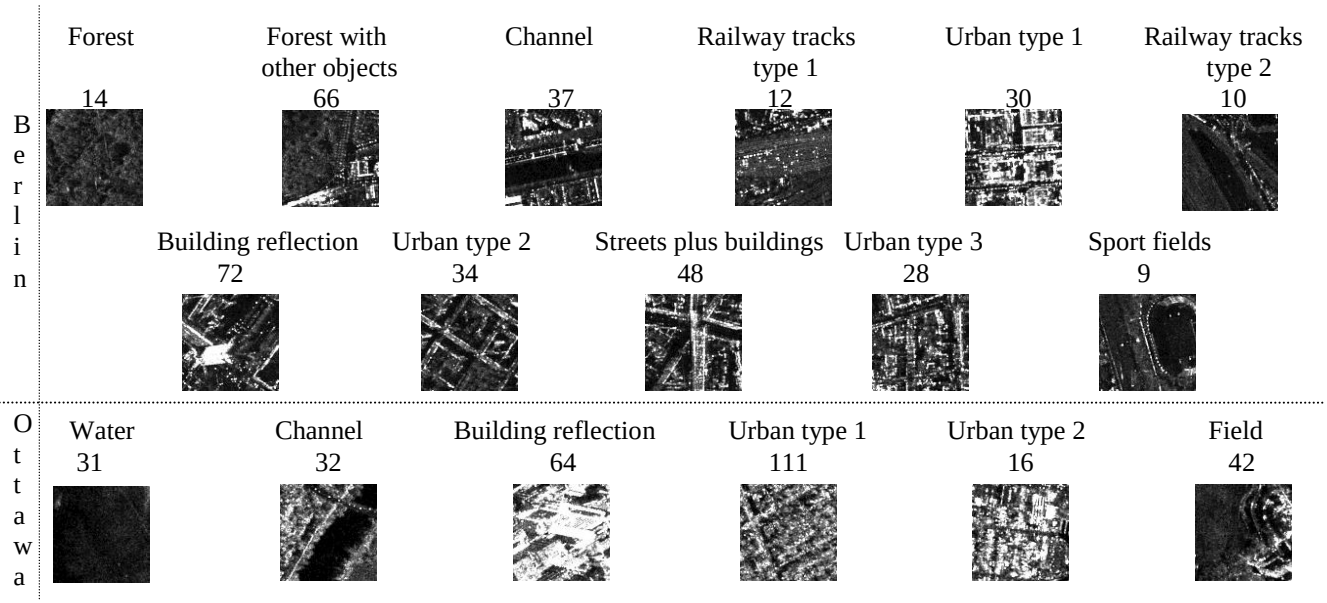

Figure 5. Typical classes that can be extracted from: the Berlin image (the top part of the figure) and the Ottawa image (the bottom part of the figure).

During the evaluation, the number of classes retrieved for Berlin area is equal to 11 and for Ottawa area equal to 6. In Figure 5 the semantic classes are presented with their corresponding number of patches in each class.

For each step (feature extraction method or incidence angle/orbit direction), we tried to detect the classes among the number of identified patches of our *test dataset*. For each class, we give 20% of the patches of each class for the training as positive examples and one patch from the rest of the classes as a negative example and we try to detect the similar patches during 7-10 training iterations. The evaluations stop when the classified patches which are displayed by the Search Engine (SVM - RF tool) remain in a stable result (no new patches are longer found from iteration to another). The procedure is repeated two times for the same class, giving the same positive and negative examples.

For the quantitative assessment, we compared the classification results with the annotated database. We propose as evaluation metric the *precision-recall* that will be computed for each class, feature, and incidence angle.

The *precision* is defined as the fraction of the retrieved images which are relevant, while the *recall* is defined as the fraction of relevant images which have been retrieved.

V. PERFORMANCE EVALUATION

This section is dedicated to the evaluation of the best features that are intended to be used for the evaluation of the incidence angles. In Figure 6 is displayed (for Berlin site with the incidence angle of 30°) the *precision-recall* for each class separately and for all four investigated features.

The average of the *precision–recall* is presented in Table I for these features computed over all the classes.

After the investigation and comparison between the features is finished the following conclusion arise that: the Gabor filters perform better than the other features especially when the *precision* is computed; regarding the *recall*, the best performance is obtained for quadrature mirror filters. The quadrature mirror filters has the advantage of being faster (in required run time for feature computation) than the Gabor filters.

TABLE I. THE AVERAGE OF THE PRECISION- RECALL

Features	Precision	Recall
GAFS 4_6	**90.11%**	49.19%
QMFS 1	78.59%	**58.77%**
GLCM 1_2_3_4	84.26%	50.70%
NLFT	71.86%	55.28%

The discussion reached a point when we have to decide what is need the *precision* that means accuracy of the relevant patches from the total number of retrieved patches or more relevant patches to be retrieved (*recall*). Because our goal is to find similar patches that exist in our *test dataset* the *recall* as a metric is considered and as a consequence of this decision the QMFS is selected from the four features investigated. The *precision* will be presented only informative in the second step where the incidence angle will be evaluate.

From the TerraSAR-X archive [34], we selected two sites that correspond to our requirements in order to have the incidence angle close to lower and upper bound of the TerraSAR-X and different orbit lookings. The range of the satellite for high resolution Spotlight mode is between 20° and 55°. These two sites are Berlin with incidence angle of 30° and 42° with ascending looking and Ottawa with incidence angle of 27° and 41° with descending looking.

In the next figures, Figure 7 and Figure 8, for these two scenes/sites the metric was computed and the results are displayed.

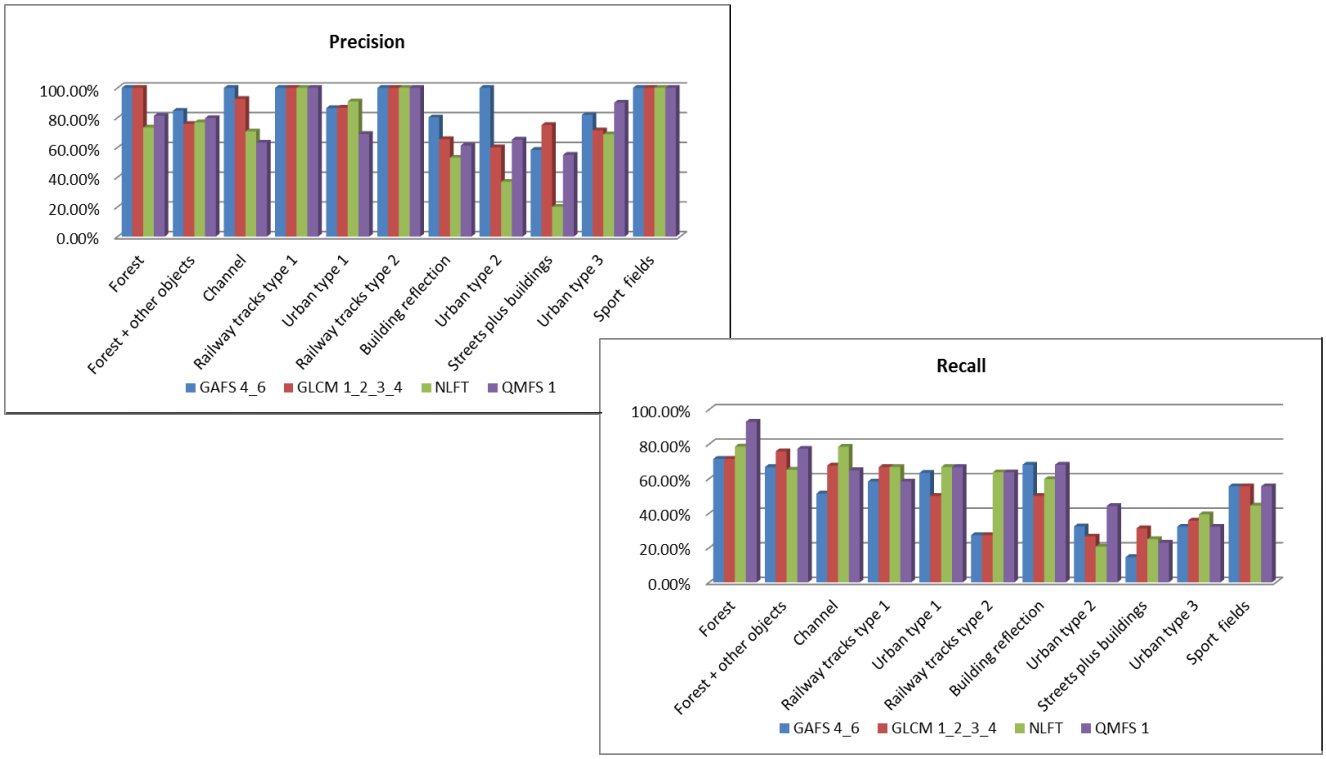

Figure 6. The results of the precision-recall for Berlin. A comparison between all primitive features (GEC-RE product, HS mode, patch size 110x110 pixels).

The best incidence angle in *recall* was obtained for both sites in the case of higher value of the incidence angle; this means a value of the incidence angle close to the upper bound of the sensor range.

This value is 42° for Berlin and 41° for Ottawa where both orbit directions ascending and descending were considered.

Evaluating the accuracy of the classification separately class by class s (the *recall* metric higher than 65%) the following observation can be noticed:

- in the case of Berlin better results are obtained for "forest", "forest plus other objects", and "building reflection" class.
- in the case of Ottawa better results are obtained for "water", "building reflection", "urban", and "field".

Another study that is presented in this section regarding the incidence angle is the influence of this parameter when both incidence angles are putted together.

There are two experiments conducted for this study: for the first one, the training was done with examples only from one case (only one incidence angle) in order to have a reference result and second time with examples from both cases (both incidence angles).

For this investigation the Berlin site is taking into account and the results are shown in Figure 9.

The average of the *recall* (marked with green color in Table II) over all the classes in both cases is:

- 32.96% when the training was done using one incidence angle (e.g. 30°),
- 38.30% when the training was done combining examples from both incidence angles.

In Table II, the accuracy of the classification presented as *precision-recall* metric is displayed. In the right side of the table, the *recall* for both cases is presented for each class separately. For eight from eleven classes the *recall* (marked with red color) is better when the training is done with data coming from both incidence angles (incidence angles that are covering the min-max range of the TerraSAR-X sensor). For the rest of the classes higher value in *recall* (marked with pink color) is obtained when the training is done only with data having the incidence angle equal to 30°.

What is interesting here for these three classes (classes: streets with some objects and different types of railway tracks) is that each of these contains objects that have a certain pattern. All these classes can be included in a more general class, namely transportation.

In both cases the class with higher *recall* (metric higher than 65%) is "forest".

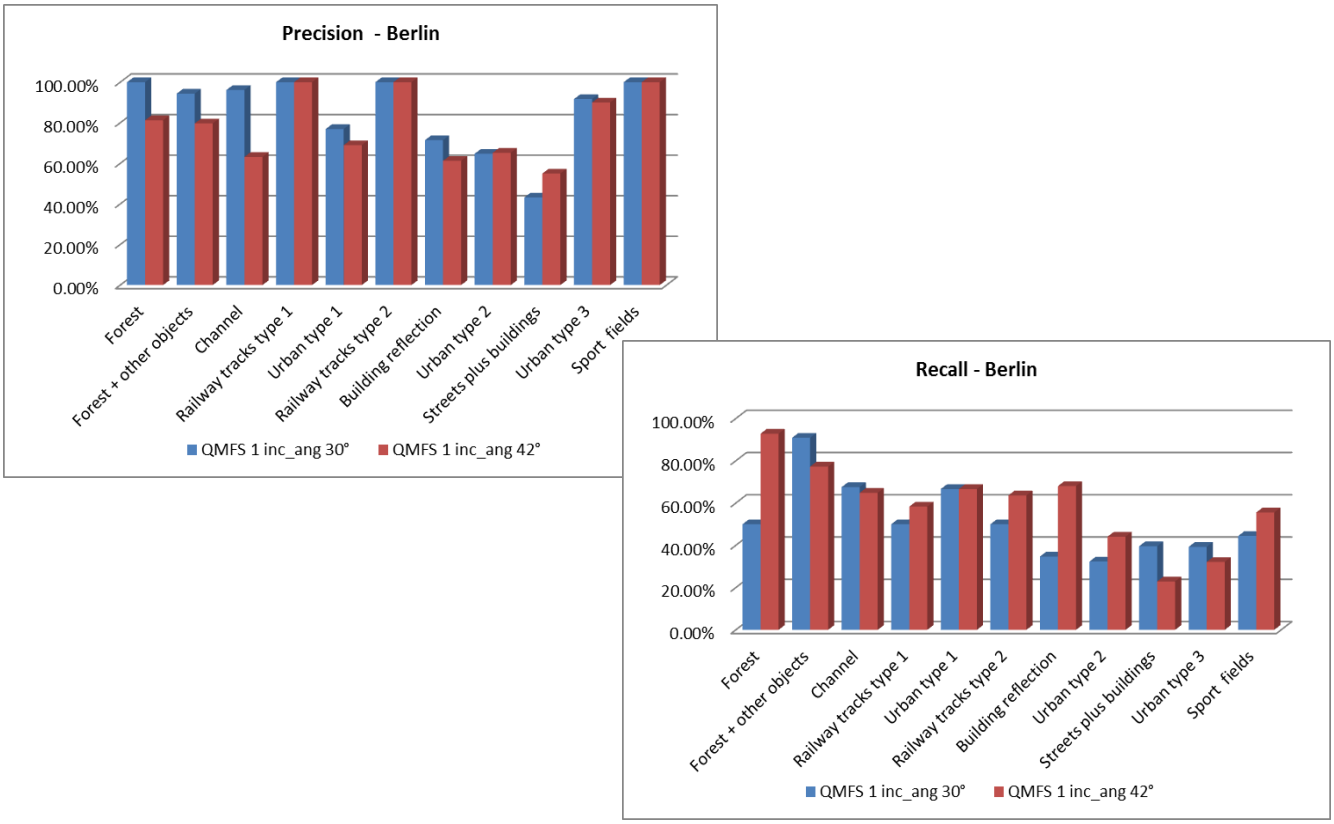

Figure 7. The results of the precision-recall for the center of Berlin. A comparison between the results obtained for both incidence angle 30° and 42°.

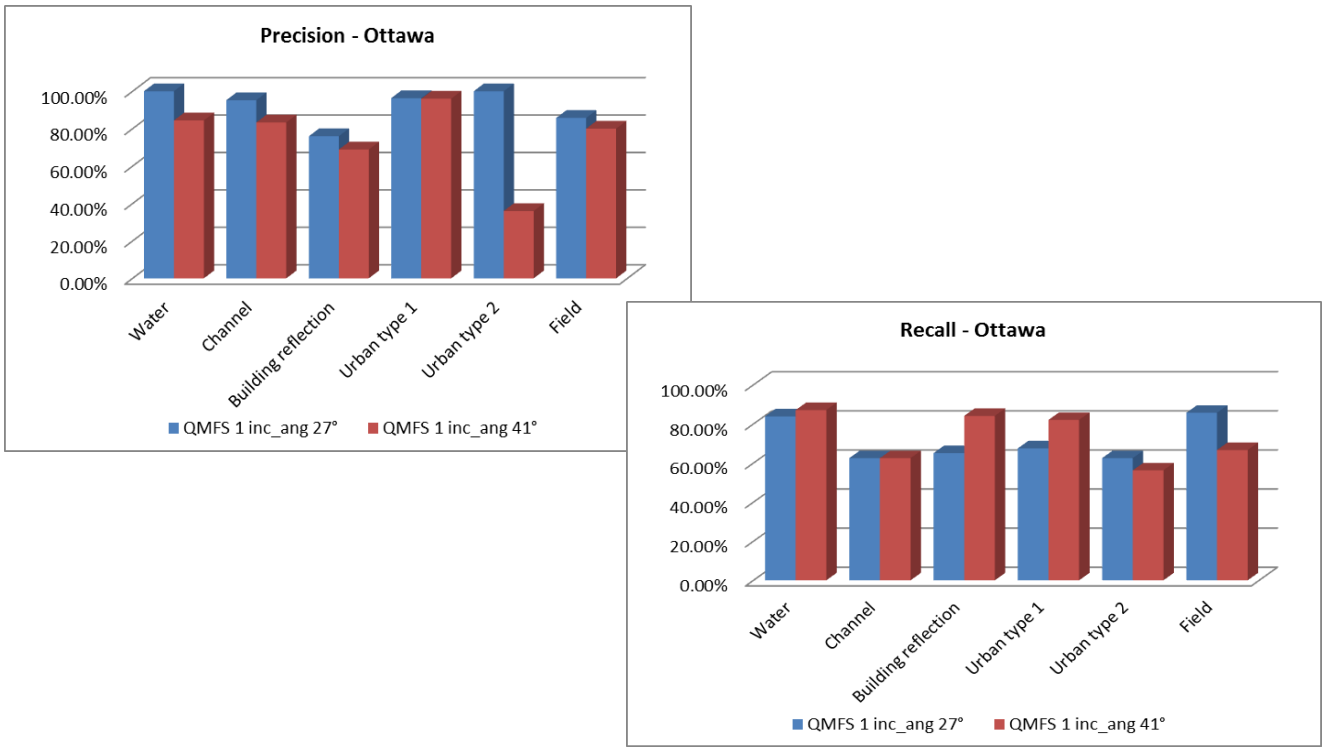

Figure 8. The results of the precision-recall for the center of Ottawa. A comparison between the results obtained for both incidence angle 27° and 41°.

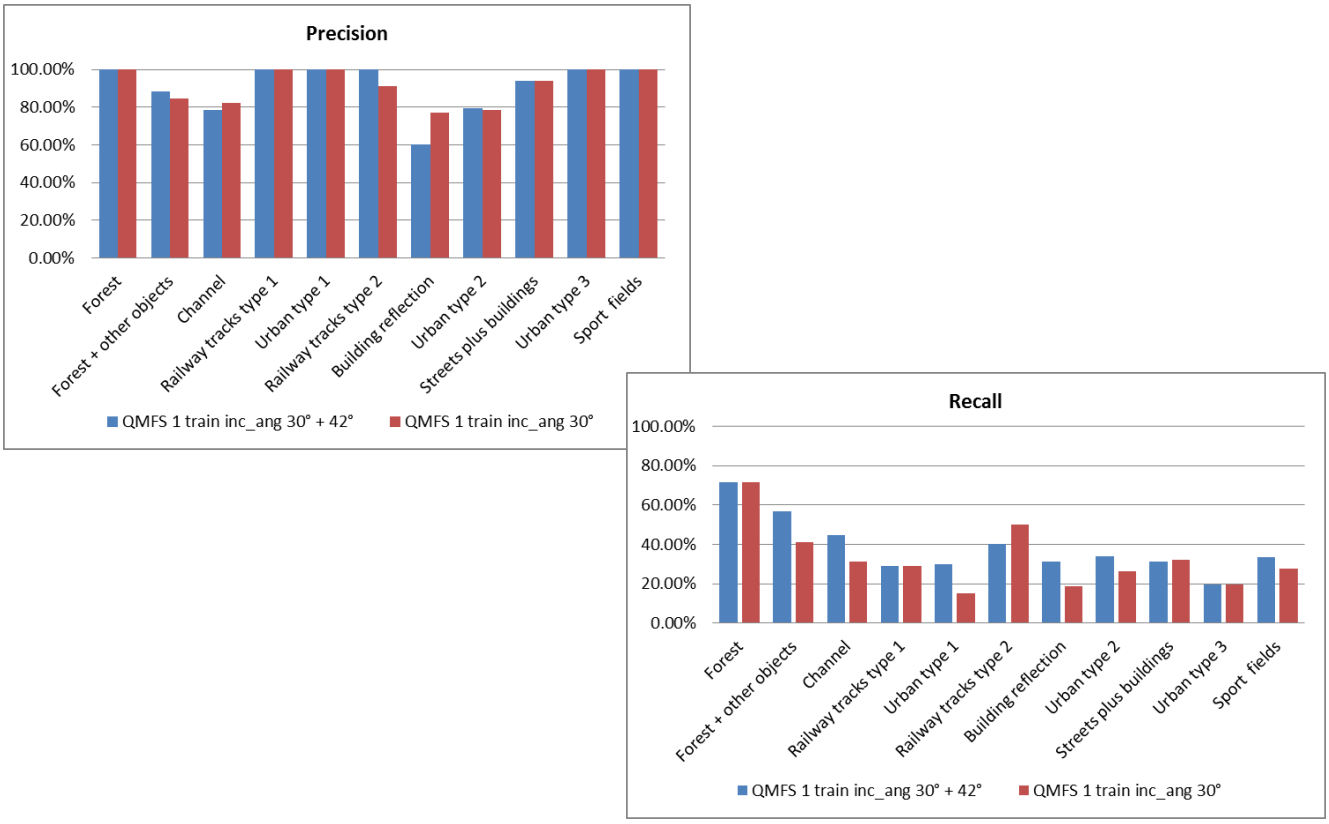

Figure 9. The results of the precision-recall in the case of Berlin. A comparison between the results when the training was done with both incidence angles (30° and 42°) and when the training was done with only one value of the incidence angle (30°).

TABLE II. A COMAPRISON OF THE PRECISION- RECALL REALISED: WHEN THE TRAINING WAS DONE WITH BOTH INCIDENCE ANGLES AND WHEN THE TRAINING WAS DONE WITH ONLY ONE INCIDENCE ANGLE IN THE CASE OF BERLIN AREA. THE FEATURES EXTRACTED ARE QMFS WITH LEVEL OF DECOMPOSITION 1.

Semantic classes	No. of patches	Precision		No. of patches	Recall	
		Incidence angle 30° and 42°	Incidence angle 30°		Incidence angle 30° and 42°°	Incidence angle 30°
Forest	28	100.00%	100.00%	14	**71.43%**	71.13%
Forest + other objects	132	88.24%	84.38%	66	**56.82%**	40.94%
Channel	74	78.57%	82.14%	37	**44.59%**	31.08%
Railway tracks type 1	24	100.00%	100.00%	12	29.00%	**29.17%**
Urban type 1	60	100.00%	100.00%	30	**30.00%**	15.00%
Railway tracks type 2	20	100.00%	90.91%	10	40.00%	**50.00%**
Building reflection	144	60.00%	77.14%	72	**31.25%**	18.75%
Urban type 2	68	79.31%	78.26%	34	**33.82%**	26.47%
Streets plus buildings	96	93.75%	93.94%	48	31.25%	**32.29%**
Urban type 3	56	100.00%	100.00%	28	**19.64%**	19.00%
Sport fields	18	100.00%	100.00%	9	**33.34%**	27.78%
Total for QMFS and all the classes		***90.90%***	***91.52%***		***38.30%***	***32.96%***

VI. TYPES OF QUERIES

The purpose of this section is to shows how to improve the state of the art of the indexing and querying systems available for Earth Observation [7], [35].

We start this section by presenting a series of query that can be asked by EO users. These queries are intended to be implemented in the next generation of our system [36]:

1) *Query for a product and its metadata:* This type of query is based on the metadata normally stored in the XML file of the TerraSAR-X [6].

"Find all GEC products, high resolution Spotlight mode with HH polarization that has the latitude equal to 52.49826 N and longitude equal to 13.3484534 E". The results of the query are presented in Table III; these parameters are extracted from the metadata of each TerraSAR-X product.

2) *Query for an image and its metadata:* This type of query is based on the image and its attached metadata (e.g., geographic latitude/longitude). This can be useful for a fast query of a location knowing the coordinates of the area [7].

"Find the images with the center of latitude equal to 45.42349 N and longitude equal to -75.69793 E and with an extension of 0.05". The result of the query gives us a list with 12 images that correspond to specified query (this type of search can be done also on the TerraSAR-X archive [7]).

3) *Query for images of products that contain patches that have certain properties*. This type of query can be divided in other sub-categories:

a) *Query by the land cover/use class of a certain patch:* This type of query is based on the metadata annotated to the patches.

"Find all patches that correspond to sport fields." The result of this type of query is presented in Figure 10 (all the patches marked with green, red, and magenta color).

b) *Query by the land cover/use class of a patch and the qualitative or quantitative spatial properties of a patch:* This type of query allows us to query for patches with some land cover/use class that are spatially related to other patches or to a user defined area.

"Find all patches containing sport fields limited in the west by the channel." The results of this type of query correspond to only one patch marked with green color in Figure 10.

c) *Query by correlating the land cover/use class of more than one patch that has various qualitative or quantitative spatial relations between them:* This type of query extends the previous query by allowing the correlation based on land cover/use class of multiple patches with various spatial relations between them.

"Find all patches that correspond to a sport field and within a distance of patches that correspond to urban area (buildings)." There are three such patches (one marked with green color and two with red color in Figure 10) that correspond to the specific query.

Another example is: "Find all patches that correspond to forest (or trees) that have in middle a sport field." The results are the patches marked with magenta color in Figure 10.

d) *Query that involves features of a patch but also other properties like the land cover/use class and spatial relations:* This type of query is based on the parameters of the feature extraction algorithms.

"Find the mean and variance of the low pass sub-band filter (the first and second value of the quadrature mirror filters vector) for a patch that corresponds to a railway tracks." This query can be useful to understand why sometimes some patches may not be grouped tougher even are containing the same object (e.g. railway tracks). Such example is found for Berlin site (Figure 5) where two classes containing railway tracks are spitted in two different classes.

In Figure 11 is presented an example showing the difference between the quadrature mirror filter (QMF) features extracted from two patches classified as bridge having the incidence angle equal to 27° and 41°.

TABLE III. THE RESULTS OF THE QUERY – TYPE 1.

No.	Product	Time UTC	Incidence angle	Orbit direction
1	GEC, SE., High Resolution Spotlight, HH	2008-10-11 05:25:17	36.08518°	Descending
2	GEC, SE., High Resolution Spotlight, HH	2008-09-30 05:25:17	35.73137°	Descending
3	GEC, SE., High Resolution Spotlight, HH	2008-09-19 05:25:16	35.73308°	Descending
4	GEC, RE, High Resolution Spotlight, HH	2009-03-23 16:43:52	30.01653°	Ascending
5	GEC, RE, High Resolution Spotlight, HH	2009-11-03 16:52:35	41.90324°	Ascending

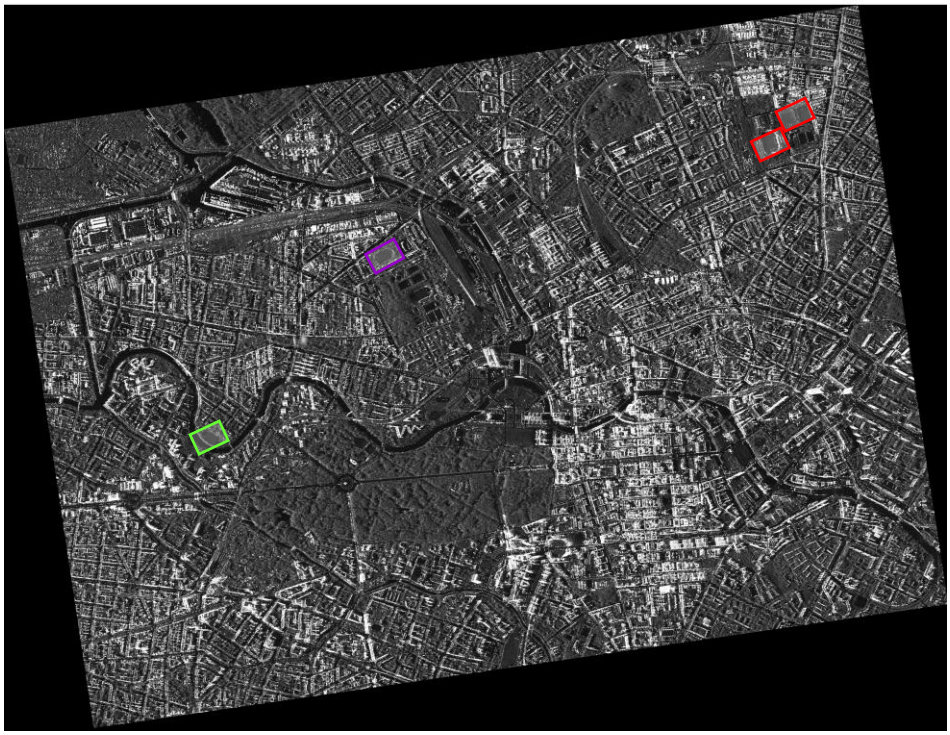

Figure 10. Results of the proposed queries (query type 3 case a), b), and c)) are marked with different color on the quick-look of the image (city of Berlin).

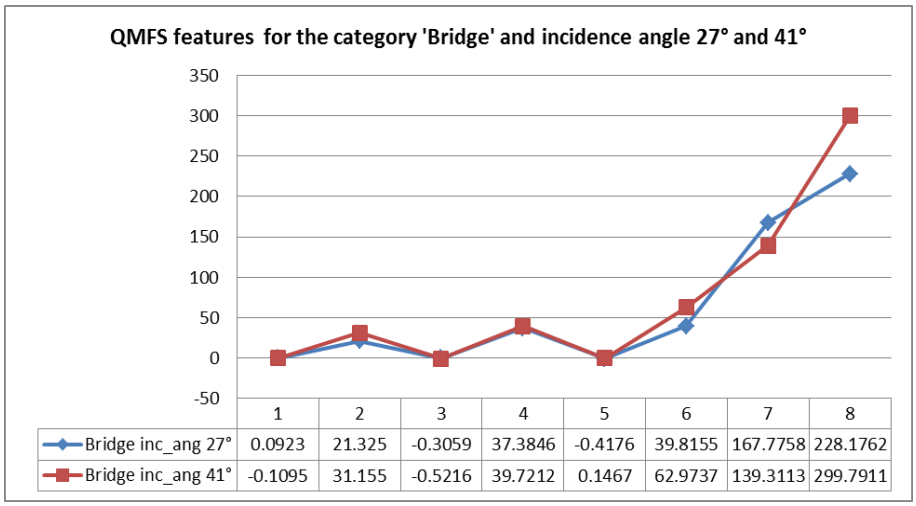

	1	2	3	4	5	6	7	8
Bridge inc_ang 27°	0.0923	21.325	-0.3059	37.3846	-0.4176	39.8155	167.7758	228.1762
Bridge inc_ang 41°	-0.1095	31.155	-0.5216	39.7212	0.1467	62.9737	139.3113	299.7911

Figure 11. Representation of the QMFS features extracted from the same patch ('bridge') having the incidence angle equal to 27° and 41° in the case of Ottawa area.

VII. CONCLUSION

Based on the results obtained in previous sections a general conclusion regarding the incidence angle can be drawn manely, the value of the incidence angle closer to the lower bound of the sensor range is optimal if the *precision* metric is considered or value of the incidence angle closer to the upper bound of the sensor range is optimal if the *recall* metric is computed. However, our goal is to retrieve similar patches in a large database and *recall* is the metric that gives as a good measure for this.

Regarding the orbit direction in both cases (Berlin and Ottawa) the classification accuracy obtained for the incidence angle was the same even the orbit looking was

different (ascending looking for Berlin and descending looking for Ottawa). This leads to the idea that the orbit direction can be disregarded because the influence of this is not so major (maybe for some classes can be important). The classification accuracy is given by the incidence angle, the parameters of the data (patch size, pixel spacing, and resolution), and the primitive features used.

As a general remark, the SAR signature depends on the incidence angle of the data and the accuracy of the classification may decrease for different values of the incidence angle.

Examining the types of queries presented in section VI, we noticed that the existing EO portals offer partial or full support for asking queries of type 1 and 2, but cannot be used to answer any of the queries of type 3 and its sub-categories. These queries can only be asked and answered if the knowledge discovery technologies are applied to TerraSAR-X images and the relevant knowledge are extracted and captured by the semantic annotations. In other words the list of queries presented above is intended to be implemented in the next generation of the system [36].

A real use case and/or application that we identified for this type of queries (e.g., type 3) is for example *"finding areas (e.g., sport terrain or field) where refugee camp or hospitals can be placed after an earthquake"* like the one in Haiti in January 12, 2010 that ZKI [37] has faced recently.

ACKNOWLEDGMENT

This work has been partially funded by ESA (European Satellite Agency) under the KLAUS project (contract no. 22823/09/I-AM).

REFERENCES

[1] C.O. Dumitru and M. Datcu, "Dependency of SAR Image Structure Descriptors with Incidence Angle", in Proc. of SPACOMM, Chamonix, May 2012, pp. 92-97.

[2] C.-R. Shyu, M. Klaric, G. Scott, A. Barb, C. Davis, and K. Palaniappan, "GeoIRIS: Geospatial Information Retrieval and Indexing System – Content Mining, Semantics Modeling, and Complex Queries", IEEE Trans. Geoscience and Remote Sensing, vol. 45, Issue 4, pp. 839-852, 2007.

[3] A. Popescu, I. Gavat, and M. Datcu, "Contextual Descriptors for Scene Classes in Very High Resolution SAR Images", IEEE Geoscience and Remote Sensing Letters, 2012, vol. 9, Issue 1, 2012, pp. 80-84..

[4] P. Birjandi and M., Datcu, "ICA based visual words for describing under meter high resolution satellite images", Proc. of. IGARSS 2009, Cape Town, 2009.

[5] P. Birjandi and M. Datcu, "Topographic independent component analysis model for under meter high resolution satellite images characterization", Proc. of ESA-EUSC-JRC_2009, Torrejon-Spanien, 2009.

[6] C.O. Dumitru, J. Singh, and M. Datcu, "Selection of relevant features and TerraSAR-X products for classification of high resolution SAR images", EUSAR 2012, Nuremberg-Germany, 24-26 April 2012, pp. 243-246.

[7] TerraSAR-X: "Basic Products Specification Document", Issue: 1.6 (TX-GS-DD-3302), 2009.

[8] R. M. Haralick, K. Shanmugam, and I. Dinstein, "Textural features for image classification", IEEE Trans. Systems, Man, and Cybernetics, SMC-3, pp. 610-621, 1973.

[9] E. Rignot and R. Kwok, "Extraction of Textural Features in SAR Images: Statistical Model and Sensitivity", Proc. International Geoscience and Remote Sensing Symposium, Washington, DC, pp. 1979-1982, 1990.

[10] A.S. Solberg and A. Jain, "Texture Fusion and Feature Selection Applied to SAR Imagery", IEEE Trans. Geoscience and Remote Sensing, vol. 35, no. 2, pp. 475-478, 1990.

[11] T. Randen and J.H. Husoy, "Filtering for Texture Classification: A Comparative Study", IEEE Trans.Pattern Analysis and Machine Intelligence, vol. 21 no.4, pp. 291-310, 1990.

[12] P.P. Ohanian and R.C. Dubes, "Performance Evaluation for Four Classes of Textural Features", Pattern Recognition, vol. 25, no. 8, pp. 819-833, 1992.

[13] GLCM, 2012, Available: http://www.fp.ucalgary.ca/mhallbey/orderliness_group.htm

[14] A.K. Jain and F. Farrokhnia, "Unsupervised Texture Segmentation Using Gabor Filters", Pattern Recognition, vol. 24, no. 12, pp. 1167-1186, 1991.

[15] L. J. Du, "Texture Segmentation of SAR Images Using Localized Spatial Filtering", Proc. International Geoscience and Remote Sensing Symposium, Washington, pp.1983-1986, 1990.

[16] J. H. Lee and W. D. Philpot, "A Spectral-Textural Classifier for Digital Imagery", Proc. International Geoscience and Remote Sensing Symposium, Washington, pp. 2005-2008, 1990.

[17] L. Shu, T. Tan, M. Tang, and C. Pan, "A Novel Registration Method for SAR and SPOT Images", Proc. IEEE International Conference on Image, pp. II.213-II.216, 2005.

[18] B. S. Manjunath and W. Y. Ma, "Texture Features for Browsing and Retrieval of Image Data". IEEE Trans. Pattern Analysis and Machine Intelligence, vol.18, pp.837–842, 1996.

[19] P. Porter and N. Canagarajah, "Robust Rotation-Invariant Texture Classification: Wavelet, Gabor filter and GMRF based Schemes", Proc. Visual Image Processing, vol. 144, no. 3, pp. 180-188, 1997.

[20] S.E. Grigorescu, N. Petkov, and P. Kruizinga, "Comparison of Texture Features based on Gabor Filters", IEEE Trans. Image Processing, vol. 10, no. 11, pp. 1160-1167, 2002.

[21] D. Zhang, A. Wong, M. Indrawan, and G. Lu, "Content-based Image Retrieval Using Gabor Texture Features", IEEE Trans. Pattern Analysis and Machine Intelligence, pp. 13-15, 2000.

[22] M. Torres-Torriti and A. Jouan, "Gabor vs. GMRF Features for SAR Imagery Classification", Proc. Int. Conference on Image Processing, Thessaloniki, vol. 3, pp. 1043 – 1046, 2001.

[23] A. Croisier, D. Esteban, and C. Galand, "Perfect Channel Splitting by use of Interpolation/Decimation/Tree Decomposition Techniques", Proc. International Conference on Information Science and Systems, Patras Greece, 1976.

[24] D. Esteban and C. Galand, "Application of quadrature mirror filters to split-band voice coding schemes", Proc. IEEE Int. Conf. ASSP, Hartford, Connecticut, pp. 191-195, 1977.

[25] P. Vaidyanathan, "Quadrature Mirror Filter Banks, M-band Extensions and Perfect-Reconstruction Techniques", IEEE ASSP Magazine, vol. 4, no. 3, pp. 4-20, 1987.

[26] A. Popescu, C. Patrascu, I. Gavat, J. Singh, and M. Datcu, "Spotlight TerraSAR-X Data Modeling using Spectral Space-Variant Measures, for scene Targets and Structure Indexing", Proc. The 8th European Conference on Synthetic Aperture Radar, Aachen, Germany, 2010.

[27] T. Zou, W. Yang, D. Dai, and H. Sun, "Polarimetric SAR Image Classification Using Multifeatures Combination and Extremely Randomized Clustering Forests", EURASIP

Journal on Advances in Signal Processing vol. 2010, ID 465612, 9 pages, 2010.

[28] M. Fauvel, J. Chanussot, J.A. Benediktsson, and J.R. Sveinsson, "Spectral and Spatial Classification of Hyperspectral Data using SVMs and Morphological Profiles", IEEE International Geoscience and Remote Sensing Symposium, Barcelona, Spain, pp. 4834-4837, 2002.

[29] R. Haralick, K. Shanmugam, and I. Dinstein, "Textural Features for Image Classification", IEEE Trans. Systems, Man, and Cybernetics, vol. 3, no. 6, pp. 610–621, 1973.

[30] M. Campedel, E. Moulines, and M. Datcu, "Feature Selection for Satellite Image Indexing", ESA-EUSC: Image Information Mining – Theory and Application to EO, 2005.

[31] A. Popescu, I. Gavat, and M. Datcu, M., "Complex SAR image characterization using space variant spectral analysis", Proc. IEEE Radar Conference, pp. 1-4, 2008.

[32] Z. Li and M. Ogihara, "Towards Intelligent Music Information Retrieval", IEEE Trans. Multimedia, vol. 8, no. 3, pp. 564-574, 2006.

[33] N. Karthikeyani Visalakshi and K. Thangavel, "Impact of Normalization in Distributed K-Means Clustering". Int. Journal of Soft Computing, vol. 4, no. 4, pp. 168-172, 2009.

[34] EOWEB portal: https://centaurus.caf.dlr.de:8443/eoweb-ng/template/default/welcome/entryPage.vm

[35] M. Wolfmueller, D. Dietrich, E. Sireteanu, S. Kiemle, E. Mikusch, M. Boettcher, "Data Flow and Workflow Organization - The Data Management for the TerraSAR-X Payload Ground Segment", IEEE Trans. Geoscience and Remote Sensing, vol. 47, no.1-1,pp. 44–50, 2009.

[36] TELEIOS project: Deliverable D6.2.1: Ontologies for the VO for TerraSAR-X data, 2012.
http://www.earthobservatory.eu/deliverables/FP7-257662-TELEIOS-D6.2.1.pdf.

[37] Center for Satellite Based Crisis Information – ZKI, 2012. Available: http://www.zki.dlr.de/article/1262.

[38] MPEG 7, 2012. Available:
http://mpeg.chiariglione.org/standards/mpeg-7/mpeg-7.htm

[39] C.O Dumitru and M. Datcu, "Study and Assessment of Selected Primitive Features Behaviour for SAR Image Description", in Proc. of IGARSS, Munich-Germany, July 2012, pp. 3596-3599, 2012.